Numerical Analysis of Nonionic Surfactant Monolayers at Water/Air Interfaces

V. Cuny,[‡] M. Antoni,[‡] M. Arbelot,[†] and L. Liggieri[§]

Université Paul-Cézanne - Aix-Marseille III, UMR-CNRS 6178 Symbio - Chimie informatique et modélisation moléculaire and UMR-CNRS 6171 Systèmes Chimiques Complexes-Thermodynamique et modélisation des milieux hors équilibre, BP 531, Av. Escadrille Normandie-Niemen, 13397 Marseille Cedex 20, France, and CNR-ICFAM, Via de Marini 6, 16149 Genova, Italy

Received: February 5, 2004; In Final Form: June 29, 2004

The time evolution of a monododecyl pentaethylene glycol monolayer at the water−air interface is investigated using velocity rescaled NVT molecular dynamics. The model we consider consists of 40 surfactant molecules and 2350 water molecules enclosed in a periodic box. The time evolution of this system is ruled by the CFF91 force field that includes intra- and intermolecular degrees of freedom for both surfactant and water molecules. The interface we consider herein is hence described in all atomic detail. We discuss the initial condition problem and study the relaxation properties to stationarity. Transient regimes of self-assembly of the surfactant chains in entangled structures in both air and water are described. From the stationary configuration, we define the interface location, determine the mass distribution across the interface, and discuss the validity of the tilt angles notion when structural roughness is considered. Using pair distribution functions, we show that, besides typical tilt angles, monododecyl pentaethylene glycol molecules might also develop domains on the interface that suggest an in-plane orientational order.

1. Introduction

The description of interface properties is one of the most important goals for the understanding of evaporation processes, aging dynamics in dispersed systems, or foam stability. Fundamental research in these domains is motivated by the determinant role of interfaces and surfactant molecules in many industrial applications. Liquid−liquid emulsions for example are widely used in industry, and their aging mechanisms are not only inhibited by usual hydrodynamical viscous forces but also by an important stabilizing effect of surfactant molecules. Their stability is known to be ruled by drop/drop coalescence mechanisms in which surfactant molecules have determinant effects.[1] The role of surfactant molecules at fluid/air interfaces also enters into play when considering evaporating mechanisms and when studying the evolution of the contact line of evaporating droplets. Foam evolution is one more applied domain in which surfactant molecules and the structure of water/air interfaces have to be understood for the description of macroscopic properties such as the balance between gravity and viscous agents.

Emulsions, evaporating systems, and foams all involve surface properties such as surface tension or surface elasticity that turn out to be sensitive to small changes in the surfactant concentration either on the interface or inside the bulk phase. These changes are linked to structural and conformational characteristics of the considered interface and can be described at the microscopic level with molecular dynamics simulations. From a fundamental point of view, adsorption and surfactant properties at liquid interfaces have been investigated for several decades. Purely theoretical and semiempirical approaches were proposed. Equations of state and adsorption isotherms have been used to study the surface activity as it pertains to surface layer coverage. In this context, two state models were recently investigated for the description of reorganization processes in adsorbed surfactant layers.[2−4]

Nonionic surfactant molecules of the alkylpolyoxyethylene glycol ether type are well dissoluble in water and constitute key compounds for detergent formulation. With the aim to describe the collective behavior and structural properties of adsorbed monolayers of such molecules, we propose to investigate in all atomic detail a monododecyl pentaethylene glycol surfactant monolayer at the water/air interface. These molecules are characterized by the general structure $H(CH_2)_nO(CH_2CH_2O)_mH$, denoted by C_nE_m, with $n = 12$ and $m = 5$ in our case. All relevant degrees of freedom are included in the atomic interactions, and both surfactant and solvent molecules are treated at the same level. Finite size effects are still not yet completely understood in such systems, and several works dealing with this problem suggest that the size of the system might be crucial for intermediate surface concentrations.[5] However, molecular dynamics simulations performed in the canonical ensemble suggest that reliable results for $C_{12}E_5$ surfactant monolayers at the water/air interface can already be obtained with 25 surfactant molecules.[6] In the following, we consider a larger number of molecules and hence assume that the number of surfactant molecules is large enough to obtain reliable statistical averages.

To prevent effects linked to micellization phenomena, the simulations were performed for molecular surface area $A = 0.64$ nm^2 that is much larger than the corresponding critical value $A_c = 0.50 \pm 0.03$ nm^2.[7] This critical area corresponds to the available area per molecule on the interface and is a characteristic parameter of $C_{12}E_5$ surfactant molecules and of their solubility in water. The different phases that appear in binary

* To whom correspondence should be addressed. E-mail: m.antoni@univ.u-3mrs.fr.

[†] Université Paul-Cézanne - Aix Marseille III, UMR-CNRS 6178 Symbio - Chimie informatique et modelisation moleculaire.

[‡] Université Paul-Cézanne Aix Aix Marseille III, UMR-CNRS 6171 Systemes Chimiques Complexes-Thermodynamique et modelisation des milieux hors equilibre.

[§] CNR-ICFAM.

10.1021/jp0494741 CCC: $27.50 © 2004 American Chemical Society
Published on Web 08/06/2004

mixtures of water and alkylpolyoxyethylene glycol ether surfactants have been described in ref 8. At water/air interfaces, due to their amphiphilic character, such surfactant molecules tend to form adsorbed monolayers.[6,9] When increasing their concentration, adsorbed surfactant molecules are spatially closer and the total energy increases due to intermolecular couplings. For $A < A_c$, the cost in energy becomes too large and the situation in which molecules are completely immersed in water becomes favorable. For $A = A_c$, surface coverage is maximal and the surfactant monolayer tends to collapse. When increasing further the surfactant concentration, coupling between dissolved molecules becomes no longer negligible and the micellization mechanism starts. A large number of molecular dynamics simulations have been performed to understand either the properties of surfactant monolayers or micellization processes. The description of the evolution of micelles in water systems has been studied in ref 10. Recent investigations of the temperature-dependent interactions of C_nE_m surfactant molecules in water have allowed a quantitative prediction of the cloud point temperature where a transition from a transparent isotropic solution into a turbid solution takes place.[11]

We consider here diluted systems where surfactant molecules adsorbed on the surface are characterized by a typical surface area $A > A_c$. In such conditions, the hydrophilic glycol chain of each molecule is completely or partially dissolved in water, while the hydrophobic alkyl chain tends to avoid the solvent and thus remains mainly in the air phase. Both alkyl and glycol chains are known to be oriented in a specific direction to the surface normal that depends on the surface concentration. Experiments have shown that in the low concentration limit alkyl chains are almost lying on the water surface and furthermore revealed a decreasing alkyl tilt angle for decreasing values of A.[12]

We arrange this paper in five parts: after the introduction section 2 lays out the model that is considered and focuses on the numerical techniques that will be used. Section 3 is devoted to the discussion of the initial condition problem, numerical methods, and relaxation to stationarity. Section 4 focuses on structural properties of the interface. We show that at surface area $A = 0.64$ nm^2 per molecule, glycol and alkyl chains of monododecyl pentaethylene glycol molecules have entangled structure and their mass distributions strongly overlap. In section 5 the characteristics of the water molecules are studied. Bond distances are shown to follow a Maxwell−Boltzmann distribution that is coherent with temperature and liquid water conditions. In section 6, tilt angles are discussed. Due to structural roughness, they take large values for both alkyl and glycol chains. In this section the existence of interface regions where preferentially oriented structures appear is also discussed. Section 7 is devoted to the conclusions of this work.

2. Model And Computational Details

The system we consider consists of a set of 40 $C_{12}E_5$ surfactant molecules adsorbed at the interface of a 2350 water molecules sample. Simulations of this system were performed with the Cerius^2 [13] package in the NVT-ensemble employing a leapfrog integration scheme.[14,15] The coupling between all atoms and molecules is derived from the CFF91 force field[16] that consists of a superposition of bonded (or covalent) and nonbonded (or steric) contributions. Intramolecular coupling constants of this force field are determined by ab initio quantum computations in the Hartree−Fock approximation for the equilibrium and distorted molecular geometries.[17] The same method has been used to evaluate atomic partial charges.[18,19] The expression of the potential that rules the evolution of internal coordinates of a given molecule is the superposition of bond, angle, torsion, and cross covalent contributions (out-of-plane contributions are neglected). To properly describe distorted configurations, harmonic contributions of the intramolecular potential have been completed with nonlinear (cubic and quartic) terms. The latter finally is written $V_b = V_{bond} + V_{angles} + V_{torsion} + V_{cross}$ with

$$V_{bond} = \frac{1}{2}\sum_i \alpha_i^{(b)}(b_i - b_{i,0})^2 \times (1 + \beta_i^{(b)}(b_i - b_{i,0}) + \gamma_i^{(b)}(b_i - b_{i,0})^2) \quad (1)$$

$$V_{angles} = \frac{1}{2}\sum_j \alpha_j^{(\theta)}(\theta_j - \theta_{j,0})^2 \times (1 + \beta_j^{(\theta)}(\theta_j - \theta_{j,0}) + \gamma_j^{(\theta)}(\theta_j - \theta_{j,0})^2) \quad (2)$$

$$V_{torsion} = \frac{1}{2}\sum_k \sum_{n=1}^{3} \alpha_{k,n}^{(\phi)}(1 + \cos(n\phi_k)) \quad (3)$$

where index i (respectively, j and k) runs over successive atom pairs (respectively, atom triplets and quadruplets). Internal coordinates b, θ, and ϕ are respectively the bond length, dihedral angle, and torsion angle variables. Constants $\alpha_i^{(b)}$, $\beta_i^{(b)}$, $\gamma_i^{(b)}$ are the bond coupling constants of atom pair number i. $\beta_i^{(b)}$ and $\gamma_i^{(b)}$ are the coupling constants of the nonlinear terms and have magnitude of order one. Nonlinear contributions are perturbations of the harmonic potential when bond length b_i is close to $b_{i,0}$ (where $b_{i,0}$ is the equilibrium bond length in a vacuum). But for distorted geometries of the molecules the latter are important for a precise description of the dynamics of the system. Notations for angle and torsion contributions are straightforward and the previous discussion holds for the nonlinearities of V_{angles}. The expression of V_{cross} is the superposition of seven cross contributions that involve bond, angles, torsion, and cross term interactions. When considering the strength of their coupling constants, one important contribution to V_{cross} rules the interaction between two successive angles and the torsion angle. It is written:

$$V_{(\theta,\theta,\phi)} = \sum_j \alpha_j^{(\theta,\theta,\phi)}(\theta_j - \theta_{j,0})(\theta_{j+1} - \theta_{j+1,0})\cos(\phi_j)$$

where ϕ_j is the torsion angle between triplet j and $j + 1$ and $\alpha_j^{(\theta,\theta,\phi)}$ is the corresponding coupling constant. One important effect of $V_{(\theta,\theta,\phi)}$ is to increase the rigidity of the molecules and hence to balance the possibility for the dynamics to develop highly distorted molecular configurations.

Nonbond coupling between atoms belonging to different molecules or between atoms of the same molecule but separated by three or more atoms is the superposition of Coulomb and 9−6 Lennard-Jones potentials. The nonbonded 1−4 interactions are scaled by a prefactor 0.5[6,9] and are computed separately. If we set the water permittivity to 1, V_{nonb} is written:

$$V_{nonb} = \sum_{i>j} \frac{q_i q_j}{r_{ij}} + \sum_{i>j} \epsilon_{ij}\left(2\left(\frac{r_{ij}^{(0)}}{r_{ij}}\right)^9 - 3\left(\frac{r_{ij}^{(0)}}{r_{ij}}\right)^6\right) \quad (4)$$

where q_i and q_j are the atomic partial charges assigned to atom i and j respectively, and r_{ij} is the interatomic distance between them. Parameters ϵ_{ij} and $r_{ij}^{(0)}$ determine the depth and the

location of the Lennard-Jones energy minimum generated by atom pair (i, j) and were computed using the Waldman-Hagler mixing rules.[20] Hydrogen bonds are supposed to be described by the combined contribution of Coulomb and Lennard-Jones forces. This important point will be checked in the following considering water molecules bond lengths.

The model that is used for water is a flexible model in which both the interatomic distances and angles evolve in time. Many models have been proposed to give an accurate description of water systems.[21] Most common models are rigid body SPC models.[22] Depending on the water phase, the bond length between hydrogen and oxygen atoms and the bond angle take specific values. For the flexible water model, we consider herein $b_{i,0} = 0.97$ Å and $\theta_{j,0} = 103.7°$. These values do not correspond to the characteristics of water in the liquid phase. But, as we will see in the following, these parameters together with the ones of nonbonded couplings[23] will yield characteristics for the water sample that are coherent with the thermodynamic conditions of the simulations.

The 40 surfactant molecules and water molecules of this system are confined in a cubic box with side length $L_x = L_y = 50.656$ Å and $L_z = 100$ Å. Water molecules are located in the lower part of this box, and the interface is perpendicular to the z-axis. Boundary conditions are periodic in both the x and y directions and the position of water molecules at the basis of the box are randomly distributed and is fixed in time. This last condition and the relatively large value of L_z are required to avoid undesired coupling between the top and the bottom of the box. Additionally, we assume that the size of this sample is large enough to guarantee the absence of coupling of the system with its own image due to periodic boundary conditions.

Computations of long-range interactions are usually the most CPU time-consuming. We use a direct atom based method. We hence restrict the evaluation of the nonbonded forces on a given atom to the contributions of the atoms within a sphere of radius 10 Å. Beyond this cutoff, nonbonded contributions are set to zero. Besides the direct cutoff method, spline methods make possible the potential to fade out slowly to zero. Although this approach allows a better description of long-range forces, we checked that simulations using this technique for the system under consideration here generate an almost frozen behavior of the glycol heads of the surfactant molecules. This effect prevents a proper description of the stationary configuration of the monolayer and shows that the relaxation process relies on the truncation procedure. The use of a direct cutoff hence acts like an external perturbing noise that helps relaxation to stationarity.[24] More sophisticated procedures for nonbonded interaction handling in periodic systems could have been used. Cutoff independent methods such as Ewald summation or fast multipole techniques are available for the treatment of long-range interactions that fade out slowly.[15,25,26] These methods have greatly raised the precision of the algorithms (in particular, conservation of total energy in microcanonical simulations) but have the drawback to consume CPU time when studying slowly relaxing behavior for large systems as the one considered herein. Other significant advances are proposed by multiple time step methods associated with Ewald summation. These techniques also allow a better treatment of molecular dynamics under periodic boundary conditions and moreover have the advantage to use large time steps without losing the simulation accuracy.[27]

Because of the use of a direct cutoff in the estimation of nonbonded coupling in our simulations, total energy exhibits a slow drifting behavior that changes the temperature of the system. To avoid this effect, we proceed as in ref 6 and rescale velocities every 50 time steps in a way to maintain the temperature of the system within the interval $T = 298 \pm 0.1$ K. We set the integration time step to 1 fs and simulate the time evolution of the system up to time 1.2 ns. The configuration of the system is stored every 300 fs for further analysis.

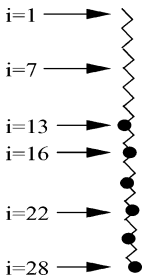

Figure 1. Index associated with the atoms of a $C_{12}E_5$ surfactant chain. The numbers indicate the indices associated with some atoms of this chain. Oxygen atoms are depicted with filled black circles. Hydrogen atoms are not displayed.

3. Initial Condition Problem and Relaxation to Stationarity

Initially, the considered $C_{12}E_5$ surfactant molecules are in an all-trans conformation. This structure is obtained from the minimization of the potential energy of a single surfactant molecules in vacuum with respect to all internal degrees of freedom. All 40 surfactant molecules were introduced following the z-direction into the water sample in a way that the first oxygen atom (the one directly linked to the alkyl chain) is located at height $z \simeq 44$ Å. The water sample is obtained from a previous run where the water molecules were simulated in a cubic periodic box of side length 50 656 Å at constant temperature $T = 298$ K during a 300 ps time period. Before introducing the surfactant molecules, the length of the box in the z direction has been extended to 100 Å and, as stated before, the water molecules at the bottom of the box were constrained to have a fixed position in subsequent runs. For this initial condition, both glycol and alkyl chains of the surfactant molecules are oriented almost parallel to the water surface normal and the polar glycol chains are completely immersed in water. To avoid numerical overflows due to overlapping molecules, water molecules that have one atom located within a distance smaller than 2.5 Å from a surfactant atom were removed from the initial configuration. Finally velocities were attributed to the atoms randomly according to a Maxwellian velocity distribution with temperature $T = 298$ K.

Although the water sample is obtained from preliminary simulations, it is clear that the linear shape of the surfactant molecules and the method used to introduce them in water make the initial condition still far from equilibrium. Therefore, before describing the details of the dynamics of the surfactant chains, subsequent runs are performed to ensure equilibration of the system. We propose to first study the equilibration time and to focus on ensemble averaged positions of the carbon and oxygen atoms of the surfactant molecules. To this end, we attribute to either carbon or oxygen atoms of a given surfactant molecule two indices k and i where $k = 1,..., 40$, is the surfactant molecule index and where $i = 1,..., 28$ is the atom number in molecule k. For simplicity, we restrict here indexation to carbon and oxygen atoms and do not consider hydrogen atoms in the study of relaxation processes. Figure 1 shows for a given molecule the numbering of the atoms.

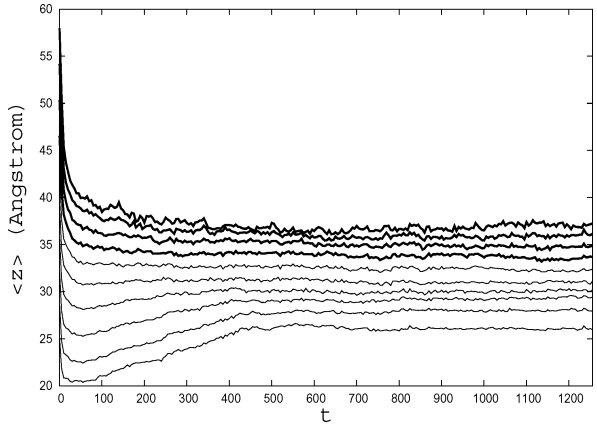

Figure 2. Evolution of average position z_i with time. The curves corresponding to carbon atoms $i = 1, 4, 7, 10$ are depicted with fat lines, whereas the ones for oxygen atoms $i = 13, 16, 19, 22, 25$, and 28 are displayed in thin lines.

We denote by $z_{i,k}$ the z-coordinate of atom number i of surfactant molecule number k. The average position z_i of atom i is then given by

$$z_i(t) = \frac{1}{N}\sum_{k=1}^{N} z_{i,k}(t) \tag{5}$$

where $N = 40$ is the total number of surfactant molecules, $i = 1,..., 28$ is the atom index, and t is time. As the system evolves, these averages will change and relax to a stationary value as shown in Figure 2. This figure indicates that in both air and water a first fast relaxation regime takes place for $t < 100$ ps. During this regime, Lennard-Jones and Coulomb forces rapidly tend to bring the system to a configuration where the atoms of neighboring molecules have positions that minimize potential energy. Beyond this time, the atoms belonging to alkyl chains have almost relaxed to a stationary configuration. Glycol chains involve much slower relaxation processes since stationarity is reached only when $t > \tau_r = 600$ ps. The latter are ruled by intermolecular processes involving neighboring surfactant and water molecules.

Although the relaxation process is slow for the glycol heads, it is noteworthy that there is a significant drifting evolution of the complete glycol chains and not only of their extremity. We explain this mobility of the glycol chains by the transfer of energy between intramolecular degrees of freedom and the environment of the atoms and by the numerical treatment of long-range couplings. The first relies on the role of bond vibrational modes that are seldom taken into account in the literature. Like angle dynamics, bond evolution depends on the local configuration of the system. It is sensitive to direct intermolecular collisions, intramolecular energy propagation in a given molecule, or by both mechanisms, for highly folded molecules. Valence bond coupling constants $\alpha_i^{(b)}$ are typically 1 order of magnitude larger than the ones (namely, $\alpha_j^{(\theta)}$) associated with angle degrees of freedom[28] and involve only two neighboring atoms. Hence these degrees of freedom are more efficient for energy transfer along the molecules than angle dynamics that is not only characterized by smaller coupling constants but also requires the displacement of three atoms. Bond dynamics hence eases energy transfer between atoms and their environment and prevents energy to be stored in specific degrees of freedom. At the scale of the system under consideration in this paper, this means that no long-standing high energy motion will take place at some location of the system since such regimes will rapidly damp due to the exchange of the excess of energy with the molecular environment. As a result, we observed that bond dynamics generates a relaxation time to stationarity that appears between 100 and 200 ps earlier. The treatment of long-range interactions and the truncation scheme used have an even more important effect on relaxation time. As stated previously, Figure 2 results from the use of a direct atom based method with a spherical 10 Å cutoff. This means that both Coulomb and van der Waals potentials are set to zero outside a 10 Å radius sphere centered on the atom under consideration. It is important to note here that the shape of the relaxation curves of Figure 2 depend on the computational method used. Different numerical treatments of long-range forces are known to modify important outputs of the simulations[29] (and references herein). As already mentioned, we checked in the present work that the discontinuity introduced by the cutoff in both van der Waals and Coulomb forces acts like a noise in the dynamics that helps relaxation to the stationary configuration.[24]

Figure 2 shows that the configuration of the system is equilibrated for time $t > \tau_r = 600$ ps. Owing to the chaotic nature of the dynamics, we can then consider that mixing is strong enough to ensure reliable time averages beyond time τ_r and hence assume that the latter coincides with usual statistical ensemble averages. Figure 2 also indicates that the thickness of the surfactant monolayer reached after equilibration is approximately 10 Å. This is much smaller value than the initial rest length of the $C_{12}E_5$ surfactant molecules computed in a vacuum that was found close to 32 Å and indicates that the surfactant molecules in the monolayer are strongly folded and/or tilted on the interface. To describe the structural properties of the surfactant monolayer at the interface, we define the interface plane location z_{int} as the stationary position of atom $i = 13$, $z_{int} = \langle z_{13}(t) \rangle$ where $\langle\ \rangle$ denotes time averaging. This definition of the interface thus relies on stationarity properties of the system and assumes the interface to be properly approximated by an horizontal plane. From Figure 2, we obtain $z_{int} \simeq 32$ Å. Simulations show that the water/air interface is a rough surface where water molecules can have a large mobility due to decreasing molecular packing. In some cases, a more refined definition of the interface might be required.[9] This is in particular recommended for detailed analysis like the water concentration profile in the three Cartesian directions at a given time. But, despite its simplicity, the definition we propose here is sufficient for our purposes since this work mainly focuses on time-averaged quantities.

4. Structural Properties of the $C_{12}E_5$ Monolayer

The thickness of the surfactant monolayer and its microscopic structure are the key points for interface characterization. Figure 3 shows a three-dimensional snapshot of the interface structure at time 1200 ps. $C_{12}E_5$ surfactant molecules are folded, and the surfactant monolayer appears as a complicated entangled system. This figure also indicates that the polar headgroups of monododecyl pentaethylene glycol molecules do not exhibit a crystal-like pattern in the aqueous phase but, similar to what occurs in the air phase, develop an entangled behavior. Instead of a clear atomic arrangement of polar heads, one can observe a highly disordered spatial configuration. This phenomenon is different from previous MD results.[6,9] Consequently, molecular arrangement in the monolayer is highly sensitive to the mobility of the atoms that is rather different in this work since all intramolecular degrees of freedom evolve in time and the numerical treatment of long-range forces is different.

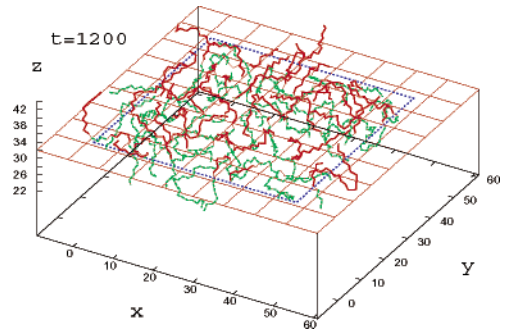

Figure 3. Snapshot of the surfactant monolayer at time $t = 1200$ ps. The plane at height $z = 32$ Å depicts the interface location and the dashed square on this plane stands for the limit of the considered periodic box. Interatomic bonds above this plane are displayed in red and the ones below are in green. Surfactant hydrogen atoms and water molecules are not displayed.

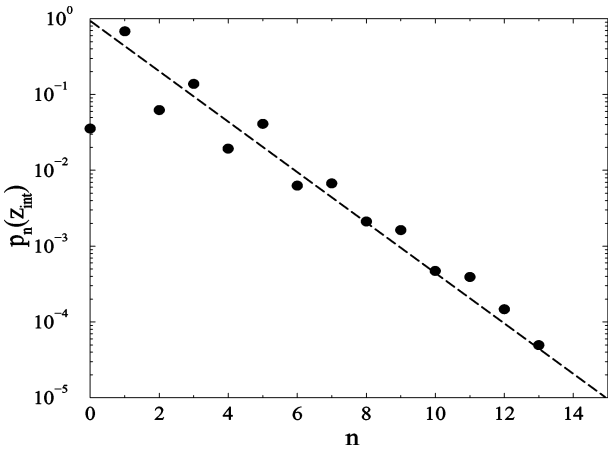

Figure 4. Intersection probability with the interface plane in a log−linear plot averaged for $t \geq \tau_r$. x-axis indicates the number of intersections with the interface plane and y-axis the corresponding probability $p_n(z_{int})$. The dashed line is shown to guide the eyes and has slope $-1/3$.

A detailed description of the interface shows configurations where the extremity of alkyl chains can be immersed in the glycol chain region or even in water. On the other hand, large sections of polar headgroups can be located above the interface plane. This effect is very similar to what occurs in water−hexane interfaces where polar headgroups might leave water and also suggests the possibility for the alkyl or glycol chains to be either moved down to the aqueous phase or up to the air phase. The description of this behavior of the surfactant molecules across the interface can be undertaken with the probability $p_n(z_{int})$ for a given surfactant molecule to cross n times the interface plane. As expected, Figure 4 shows that the most probable situation corresponds to events in which surfactant chains have a single intersection with the interface plane with probability $p_1 \simeq 0.68$. But, as $p_0 \simeq 0.04$, this figure also shows that surfactant molecules might also have a non-negligible probability to be either completely below or above the interface plane. This effect is linked to the fact that in the stationary regime, microscopic dynamics of the system can lead to situations in which surfactant chains might switch above and below the interface plane. Figure 4 moreover shows that surfactant molecules can have several intersections with the interface with exponential-like decreasing probability for large values of n. This possibility of a relatively large number of intersections with the interface is a signature of the strong disorder that occurs in the position of the attachment point of both glycol and alkyl chains.

As shown in Figure 3, the distortion of the surfactant molecules leads to a complex structure of the monolayer that can be characterized with the Shannon entropy. We thus define at height z the entropy $s(z)$ by

$$s(z) = -\sum_n p_n(z) \ln(p_n(z)) \qquad (6)$$

For $t > \tau_r$, the shape of $s(z)$ is an almost uniform distribution in the range $z \in [26\text{ Å}, 40\text{ Å}]$ and is zero elsewhere. For all values of $z \in [26\text{ Å}, 40\text{ Å}]$, we checked that the probability distribution $p_n(z)$ is almost similar to the one displayed in Figure 4 but with a faster decreasing probability for large intersection number n. This indicates that the disorder inside this z-range has similar characteristics and extends over almost the complete width of the monolayer. As a result, the dynamics generates distorted configurations over the complete length of the surfactant molecules and not only at their extremities.

Another possible way of assessing interface structure is in terms of the mass distribution of alkyl/glycol chains and water. To some extent, the previous discussion and Figure 2 already suggested that both glycol and alkyl chain mass density distributions might overlap since glycol chains can be squeezed out of the water toward the alkyl chain domain and alkyl chain pushed down to the water phase. The mass density distribution across the interface shown in figures 5 clearly illustrates this effect. It also indicates that a non-negligible proportion of the polar chain distribution is outside the water sample and that the hydration region is confined between $z = 23$ Å and $z = 31$ Å.

As the distributions of Figure 5 are obtained from simulations that rely on a full description of inter- and intra-atomic degrees of freedom, they contain all possible contributions to the layer properties, including surface structural roughness and strong out-of-equilibrium dynamical fluctuations. The alkyl mass density distribution of Figure 5a is close to a Maxwellian distribution, whereas the glycol one seems to be a superposition of two such distributions. The estimation of the glycol chain (respectively, alkyl) thickness is obtained in the following from the full-width σ_g (respectively, σ_a) at height 1/e of a Maxwell interpolation of the glycol (respectively, alkyl) distribution of Figure 5b.[30] The interpolated distributions of Figure 5a are represented in Figure 5b and give respectively, $\sigma_g = 7.3$ Å and $\sigma_a = 8.0$ Å. To our knowledge, no experimental data are available for the mass density distribution of $C_{12}E_5$ monolayers when $A = 0.64$ nm^2. Near the cmc of such monolayers ($A = 0.50$ Å^2) experimental observations show that the intrinsic layer thickness of the glycol (respectively, alkyl) chain region is $\sigma_g^{exp} = 13.5 \pm 2$ Å (respectively, $\sigma_a^{exp} = 14 \pm 2$ Å).[7] Although surface areas are different, this however suggests a too important discrepancy of the numerical values obtained in this article with experimental data. One explanation might be the parameters of the CFF91 force field that attribute coupling constants that are too small to angle dynamics. Another reason invokes the role of structural roughness of the interface that clearly appears in this work and that is not included in the capillary wave model of a pure liquid in which correlations between the conformation of the chains and roughness is neglected.[31] Consequently, roughness and intrinsic thickness might not add in quadrature. Model capillary waves corrections to experimental data might underestimate structural roughness and hence give an overestimated thickness of alkyl and glycol layers. Still, the thickness of the alkyl (respectively, glycol) layer are significantly smaller than the fully extended chain 14 Å (respectively, 18 Å). This is due to

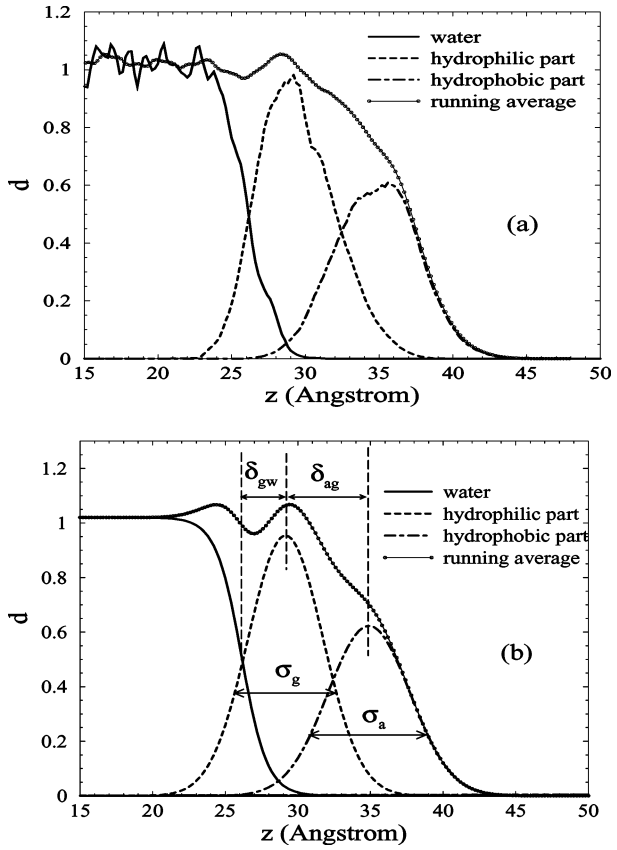

Figure 5. (a) Average mass density distribution in the *z*-direction obtained for $t > \tau_r$, and (b) interpolated curves resulting from a Maxwellian fitting of both alkyl and glycol distributions and a hyperbolic tangent interpolation of the water distribution. Total mass distribution obtained from a running average is shown by a black-dotted line. δ_{ag} (respectively, δ_{gw}) is the distance between the centers of the alkyl (respectively, midpoint of the water distribution) and glycol chains distributions. σ_g (respectively, σ_a) are the full width at height 1/e of the glycol (respectively, alkyl) interpolated distribution.

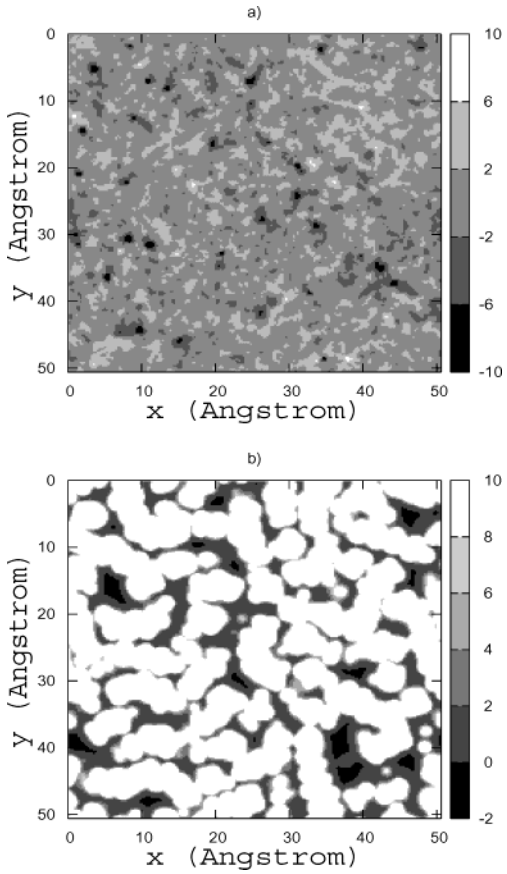

Figure 6. (a) (respectively, (b)) Coulomb energy truncated between ±10 eV (respectively, van der Waals truncated between 10 and −2 eV) at time $t = 600$ ps and height $z = z_{int} = 32$ Å. Gray scale indicates the value of the energy in eV and are identical for both figures.

both the distortion of the chains and their tilted behavior away from the normal to the interface.

Other key parameters for the description of structural properties of the surfactant monolayer are the separation of the distributions. These parameters show to which extent distributions of Figure 5 overlap. From Figure 5b we obtain $\delta_{ag} \simeq 5.8$ Å and $\delta_{gw} \simeq 3.0$ Å. The overall mass density distribution is the superposition of all mass density contributions and leads to a total mass density profile that looks similar to experimental observations obtained for $C_{12}E_m$ surfactant with $m = 2$, $m = 4$, and $m = 6$ but at higher surface concentration.[32] Finally, Figure 5 shows that there is almost no water in the alkyl chain region. This is in agreement with neutron reflection experimental data for water/air interfaces with C_nE_m surfactant molecules.[30]

Figure 5 also allows the characterization of the overlap of the distributions. We define by τ_{gw} (respectively, τ_{aw}) the surface fraction of the glycol (respectively, alkyl) mass distribution with water and by τ_{ag} the surface fraction of the alkyl mass distribution with the glycol mass distribution. From the data of Figure 5b we get $\tau_{gw} = 19\%$, $\tau_{aw} = 2\%$ and $\tau_{ag} = 38\%$. The large value of τ_{ag} indicates that the entanglement of the surfactant molecules leads to an important overlap of the hydrophobic and hydrophilic domains of the monolayer. On the other hand, the nonzero value of τ_{aw} shows that hydrophobic chains can also come in close contact with the water sample. In this situation, alkyl chains are almost lying on the interface. From the value of $\tau_{gw} = 19\%$, it turns out that only three ethelyne groups over five of the monododecyl pentaethylene glycol molecules contribute to anchor the molecules in water.

Figure 6 displays the Coulomb and van der Waals (vdW) energy distribution at the interface location at time $t = 600$ ps. Both figures show a complicated spatial dependence, and no regular pattern shows up either in the Coulomb profile or in the van der Waals one. As time goes on, these patterns evolve according to the dynamics of the molecules, but no qualitative modifications are observed. The typical size of the patterns remain for example the same although their distribution is changing. Figure 6a shows that Coulomb energy is close to zero in a large part of the interface due to the shielding of the electric field. Larger values of Coulomb energy appear as small black or white spots and indicate the location of an atom near the grid point used to build the figure. Figure 6b shows that the vdW energy is essentially positive due to the important packing of the atoms and to the rapidly diverging behavior of the vdW potential for distances $r < r_{ij}^{(0)}$. However, small domains of typical size 3×3 Å where the vdW energy is negative still exist on the interface. This means that there is still room for small molecules to be adsorbed on the interface. When investigating the shape of the energies for $z < z_{int}$ the Coulomb energy profile remains very similar to the one of Figure 6b, whereas vdW energy profile is diverging everywhere due to dense packing. For $z > z_{int}$ both Coulomb and vdW profiles vanish progressively when leaving the sample and for $z = 45$ Å the energy is almost zero.

Figure 7 displays a 3D plot the nonbonded energy V_{nonb}. Due to the very localized divergences Coulomb energy, this figure

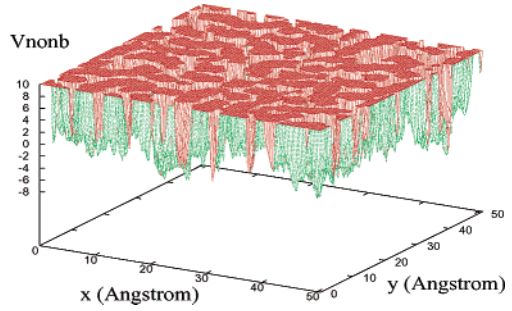

Figure 7. 3D plot of the energy surface at height z_{int} and time $t = 700$ ps truncated between -2 and $+10$ eV.

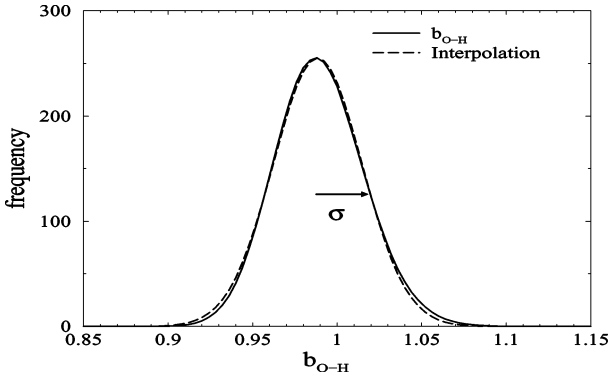

Figure 8. Histogram of b_{O-H} distances between oxygen−hydrogen atoms in water molecules (fat line) together with a Maxwellian interpolation of the histogram (dashed line). Vertical scale is arbitrary. This histogram is constructed with $N = 500$ histogram bars over range 0.85 Å $< b_{O-H} <$ 1.15 Å and σ is the standard deviation associated to the Maxwellian fitting.

can be seen in first approximation as the 3D plot of vdW energy of Figure 6b. This figure shows the complex energy distribution and the compactness on the interface. When approaching a test particle from the air side, it will first be affected by vdW coupling. Electrostatics also enters into play but only when the test particles are close enough to the interface for the local electrostatic field of the molecules to be no longer shielded. Beside vdW forces, Coulomb potential contributes then significantly to the interatomic force.

5. Characteristics of Water

Figure 5b indicates that the considered water model leads to an average mass density $d(z) = 1.03$ in the pure water phase. This is 3% larger than expected and can be explained by either the possibility of coupling constants that are too small for water molecules in the force field or by the anisotropy of the system in the neighborhood of the interface that is known to generate resulting downward oriented forces. Precise explanation of this phenomenon is out of the scope of this paper. It is however important to check whether the characteristics of water molecules are coherent with liquid water in the temperature conditions of the system.

Figure 8 shows the histogram of bond distances b_{O-H} between oxygen and hydrogen atoms in water molecules. This histogram is computed using all the water molecules and averaged over time for $t > \tau_r$. It is centered on a value 0.99 Å that is larger than the rest distance between oxygen and hydrogen water molecules that was set to 0.97 Å in the force field. This bond stretching is a consequence of water molecule coupling due to nonbonded interactions in the solvent. For the water angles distribution one gets a figure that is qualitatively similar to Figure 8 but with a typical value of 99°. Conversely to bonds lengths, bond angles in the water phase are narrower than the rest bond angles given by 104.5°. This effect is known for flexible models (see ref 21 for an extensive and detailed discussion about water models) and due to the formation of hydrogen bonds that tend to relax the angles to smaller values. The consequence of bond length stretching and bond angles narrowing is a significant increase of the dipole moment of the water molecules. This enhancement of the dipole moment might lead to undesirable effects linked to dense packing in the bulk that are not observed experimentally.[33] However, in the neighborhood of the interface, larger dipolar moments due to the anisotropy between liquid and gaseous water cannot be excluded. A more favorable alignment of the dipolar moments together with the vertical downward resulting force then explains the larger mass density of water.

We consider the standard deviation σ of the interpolating Maxwellian curve of Figure 8 as a reliable parameter for bond fluctuation characterization. From the fitting, we get $\sigma \simeq 3.0 \times 10^{-2}$ Å. The corresponding fluctuations in the value of the potential energy of a single O−H bond gives $V_{bond}(\sigma) = 3.26 \times 10^{-21}$ J. When comparing this value with the one due to thermal fluctuations, $k_B T = 4.11 \times 10^{-21}$ J where k_B is the Boltzmann constant and $T = 298$ K the working temperature, we observe that both values have the same order of magnitude. The same result shows up for angle distribution where $\sigma \simeq 5.5°$ and $V_{angle}(\sigma) = 3.11 \times 10^{-21}$ J. Obviously, this observation is true for all the contributions to the potential energy since the runs are performed in the NVT ensemble and energy equipartition should be verified for all degrees of freedom when $t > \tau_r$. As simulations are canonical, fluctuations of the different contributions to the potential energy also have to compensate each other in a way to maintain the temperature constant. But it is of fundamental interest to emphasize here the fact that time evolution of bond lengths and angles yields time averages derived from numerics that are coherent with thermodynamical expectations. This last observation also confirms that the stationary behavior of the system described in section 3 can be considered as being sufficiently relaxed for time averages to be relevant.

6. Tilt Angles

Alkyl and glycol tilt angles ($\theta_{a,k}$, $\theta_{g,k}$) are defined in Figure 9. In estimating the typical tilt angles of folded molecules one is faced with an ambiguity in their definition. Besides the problem of assigning a clear geometry to distorted and flexible molecules, the definition of tilt angles is ambiguous due to structural roughness and to the dependence of angles and chain conformation with surface coverage. In section 3, we mentioned that one simple way to determine interface location is to consider the ensemble and time-averaged position of atom number 13 given by the value of $\langle z_{13} \rangle = z_{int}$ when $t > \tau_r$. In doing so, we define an interface plane of constant height $z_{int} \simeq 32$ Å and considerably simplify, by smoothing out all dynamical fluctuations, the actual complexity of the interface. Using this interface plane, the tilt angles for a given surfactant molecule can be calculated with the alkyl (respectively, glycol) vector that links atom 1 (respectively, 28) to a reference atom m that is the nearest atom (hydrogen atoms excluded) of the considered molecule to the interface. The use of reference atom m brings up the question of the uniqueness of the definition used for tilt angles. As already stated in section 4, surfactant molecules might have more than one intersection with the interface plane and, although the probability for a single crossing is the largest, the statistical

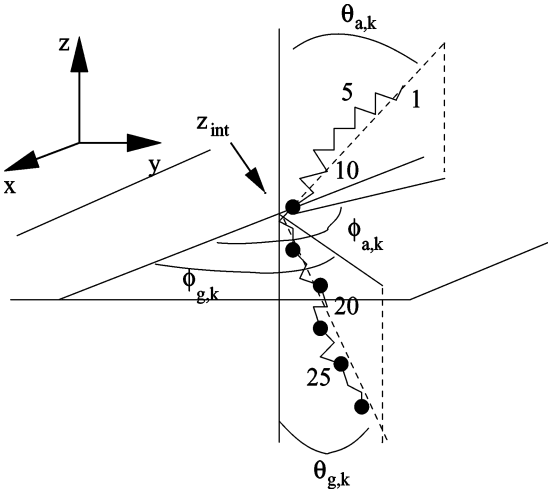

Figure 9. $C_{12}E_5$ surfactant chain number k. Angles $\theta_{a,k}$ and $\phi_{a,k}$ are defined as the polar and azimuth alkyl angles whereas $\theta_{g,k}$ and $\phi_{g,k}$ are the polar and azimuth glycol angles. Oxygen atoms are depicted with filled black circles. Hydrogen atoms are not displayed. The horizontal plane indicates the interface location at $z_{int} \simeq 32$ Å. The numbers have the same definition than in Figure 1.

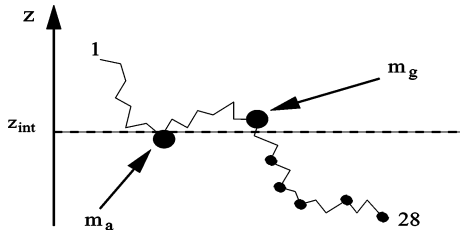

Figure 10. Location of atom m defined as the nearest atom of the considered surfactant molecule to the interface plane z_{int}. Atoms m_a and m_g are shown with a large black point. Small black points refer to oxygen atoms and numbers have the same definition as in Figure 1. m_a is the first atom of a given surfactant molecule below the interface when running along the molecule from atom 1, and m_g is the first atom above the interface when running along the molecule from atom 28.

weight of multiple intersection situations cannot be neglected (see Figure 4). Figure 10 displays for example the configuration of a surfactant molecule having two intersections. In this case, the tilt angles can be deduced from either reference atom m_a or m_g. In the following, the reference atom for the computation of the angles is m_g. If we denote by m this reference atom, one gets for molecule number k:

$$\theta_{a,k} = \arccos\left(\frac{z_{1,k} - z_{m,k}}{|r_{1,k} - r_{m,k}|}\right) \tag{7}$$

where $r_{i,k} = (x_{i,k}, y_{i,k}, z_{i,k})$ is the location of the ith atom of molecule number k. The same definition is used to evaluate the glycol tilt angle $\theta_{g,k}$ but, instead of atom 1, we consider atom 28. More refined definitions of the tilt alkyl angle can be used. One possibility is to compute the latter from the angles of all atoms having an index smaller than the reference atom m:

$$\bar{\theta}_{a,k} = \frac{1}{m}\sum_{p=1}^{m} \arccos\left(\frac{z_{p,k} - z_{m,k}}{|r_{p,k} - r_{m,k}|}\right) \tag{8}$$

with m $\neq$ 1. The ensemble averaged alkyl tilt angle $\theta_a(t)$ is finally defined by $\theta_a(t) = 1/N\ (\sum_{k=1}^{40})\theta_{a,k}(t)$. The same definition is used for $\theta_g(t)$. Figure 11 shows the evolution of θ_a and θ_g. We retrieve the typical relaxation times already discussed in section 2 since θ_a relaxes to an almost stationary value for $t \approx 100$ ps while θ_g requires time $\tau_r \simeq 600$ ps to be equilibrated. A comparison of both θ and $\bar{\theta}$ is given in Table 1 after averaging over time.

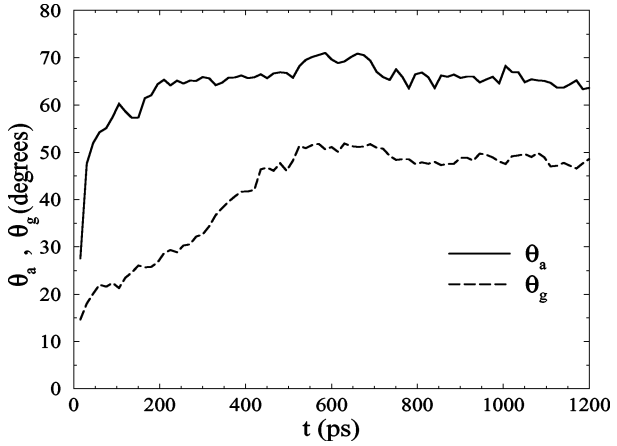

Figure 11. Running averages of both θ_a (full curve) and θ_g (dashed curve). Time averaging window was set to 50 ps in this figure.

TABLE 1: Average Values of Alkyl and Glycol Tilt Angles for the Three Definitions θ, $\bar{\theta}$, and $\tilde{\theta}$

θ_a	$\bar{\theta}_a$	$\tilde{\theta}_a$	θ_g	$\bar{\theta}_g$	$\tilde{\theta}_g$
63°	57°	59°	51°	55°	50°
±5°	±3°	±3°	±3°	±2°	±3°

The surfactant glycol groups are usually believed to be almost vertically anchored in water and confined in the half space below the first oxygen atoms.[6] For the force field and the simulations scheme used in this work, Figure 3 already demonstrated that this was not the case. Figure 11 furthermore shows that $\theta_a \simeq 63° \pm 5°$ for $t > \tau_r$. This large value and its relatively fast relaxation to stationarity are a consequence of the large molecular surface ($A = 0.64$ nm^2) that allows the alkyl tails to evolve in space and moreover suggests that new degrees of freedom such as bond length fluctuations do not enter significantly into play for the alkyl chains dynamics. This is clearly not the case for the glycol chains. It shows up from Figure 11 that for $t > \tau_r$, θ_g converges to stationary value $\theta_g \simeq 51° \pm 3°$ that is far outside the expected range obtained in fixed bond molecular dynamic simulations.[6] Such a large value of θ_g is a signature of the enhanced mobility of the glycol chains due to energy transfer between intramolecular degrees of freedom and the environment of the atoms. It also indicates that the stationary configuration of the glycol chains relies on the description accuracy of internal degrees of freedom and of the numerical technique, in particular, the direct cutoff for long-range coupling truncation. Similar figures are obtained when considering definition of eq 8 of the tilt angles and defining by $\bar{\theta}_a(t) = 1/N(\sum_{k=1}^{40})\ \bar{\theta}_{a,k}(t)$ the average alkyl tilt angle. Values of tilt angles are collected in Table 1 where $\tilde{\theta}$ is a third definition of the tilt angle given by

$$\tilde{\theta}_a = \arccos\left(\sqrt{\frac{1}{N}\sum_{k=1}^{N}\cos^2(\theta_{a,k})}\right) \tag{9}$$

Due to the high distortion of the surfactant molecules, all the definitions of tilt angles give values that are in agreement as shown in Table 1.

Figure 12 shows the alkyl and glycol angles distribution functions averaged over time $t > \tau_r$. Both have a broad shape that extends over a large angle range. This illustrates again the fact that alkyl and glycol chains are rather bulky and moreover

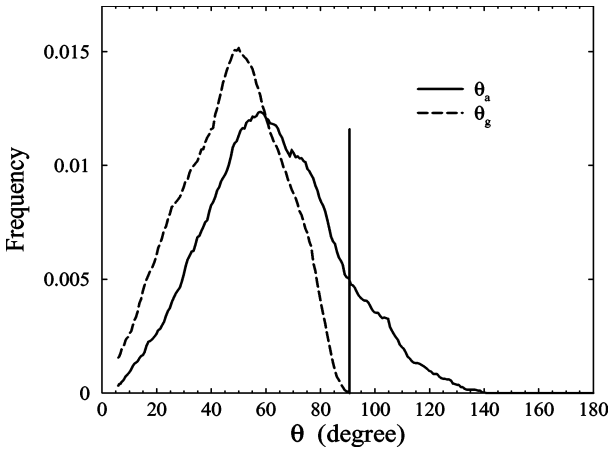

Figure 12. Time averaged distribution of θ_a (full curve) and θ_g (dashed curve) over time range $t > \tau_r$. Vertical line indicates angle 90 degrees.

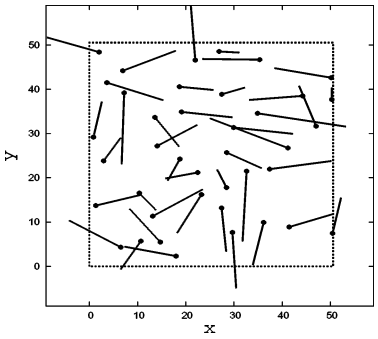

Figure 13. Snapshot of the projection of alkyl vectors in the interface plane ($z_{int} \simeq 32$ Å) at time $t = 1200$ ps. The dashed square shows the limit of the considered periodic box. Points indicate the location of atom m_g.

that the tilt angle of alkyl vector can become larger than 90 degrees. This is a consequence of the possible penetration of alkyl chains inside the glycol chain region as already discussed in section 4. We hence retrieve here overlapping characteristics between the hydrophobic and hydrophilic part of the monolayer due to the folding and to the entangled behavior of the surfactant molecules in the monolayer.

One important point is to determine whether an ordered-like structure still persists with the model interface considered here. Figure 13 depicts the projection in the (x, y) plane of the alkyl vector that was defined as the vector linking carbon atom 1 with atom m_g. It appears that the dynamics tends to align the section of the surfactant molecules lying above the interface. This phenomenon clearly shows up in the upper right part of Figure 13 where several neighboring molecules are oriented in a direction that is close to the x-axis direction. This effect results from the combined contribution of Lennard-Jones and Coulomb intermolecular interactions. Due to their long-range nature, nonbonded forces tend to bring molecules together or to push them apart. For close enough molecules, the local behavior of the electrostatic field due to atomic relative charges and repulsive van der Waals effect will prevail in the evolution of the atoms. Figure 13 suggests that the interplay of both Lennard-Jones and Coulomb interaction yields on average a coupling that allows neighboring molecules to be trapped in their respective potentials. Complete molecules or only parts of them might hence develop long-lived synchronized motion within their neighborhood.

With the aim to describe the apparent ordering of the alkyl vectors of Figure 13, we evaluated the time evolution of the probability distribution $g(\phi_a)$ to observe a given angle ϕ_a at given

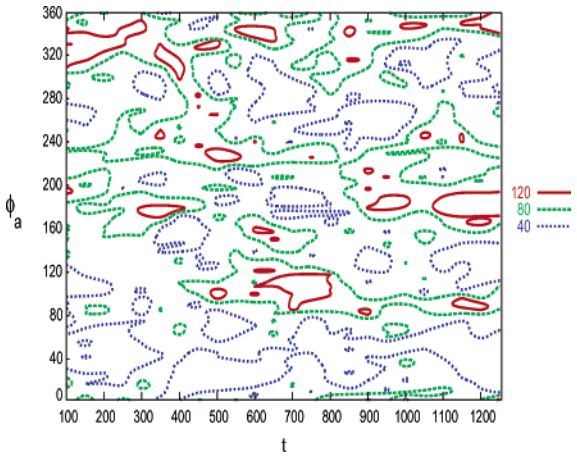

Figure 14. Contour plot of angle distribution function $g(\phi_a)$ as a function of time for $t > 100$ ps. Full lines stand for the contours where $g(\phi_a) = 120$, long-dashed contours are for $g(\phi_a) = 80$, and short dashed lines are for $g(\phi_a) = 40$.

time t. Distribution $g(\phi_a)$ indicates the frequency to obtain events in which surfactant alkyl vectors take the value $\phi_{a,k}$ within angles range $[\phi_a, \phi_a + \delta\phi_a]$ where $\delta\phi_a = 2\pi/100$. In the previous section, we noticed that the dynamics of the interface is relaxed for $t > \tau_r$. But as far as alkyl chains are concerned, Figure 2 shows that stationarity is already reached for $t \approx 100$ ps. We can hence reasonably investigate alkyl vector properties earlier than τ_r. Figure 14 shows a contour plot of $g(\phi_a)$ for $t \geq 100$ ps, resulting from sampling periods of 10 ps. For clarity, only three smoothed contour levels are represented. This figure indicates that the alkyl angle distribution is far from uniformity and exhibits patterns reminiscent of the peaks and wells appearing in the time evolution of $g(\phi_a)$. The closed domains of this figure are statistically relevant and emphasize time intervals where the dynamics supports given values of angles ϕ_a. Full contours indicate angular domains where value ϕ_a has largest probability to appear. Figure 14 suggests for example that ϕ_a preferentially takes values close to either 180° or 360° at time $t = 1200$ ps. This is coherent with the orientations observed in Figure 13 and shows that synchronization of neighboring alkyl chains close to angles 180° or 360° observed in this figure, already started at time $t = 1100$ ps and persists beyond the simulation time.

The previous discussion illustrates that equilibrium of $C_{12}E_5$ surfactant chains are characterized by a complex entangled structure. The water/air interface hence experiences a large number of molecular configurations that are ruled by both inter- and intramolecular degrees of freedom. Even though the conformation is stationary, Figure 14 demonstrates that the alkyl vector tilt angle distribution function $g(\phi_a)$ cannot be reduced to a uniform law. Another way to evidence orientational order is to consider the angle differences of neighboring surfactant molecules. We define to this end the relative differences $\Delta\theta_a = \theta_{a,k} - \theta_{a,j}$ and $\Delta\phi_a = \phi_{a,k} - \phi_{a,j}$, where surfactant molecule j is the nearest neighbor of surfactant molecule k at a given time.[34] Figure 15 displays the shape of the probability to find a given value of $\Delta\phi_a$. To smooth out dynamical fluctuations, curves are obtained from an average over time sequences. For $t \in$[650 ps, 700 ps] (respectively, $t \in$[1000 ps, 1050 ps]) alkyl chains of neighboring molecules tend to be preferentially oriented in the same direction (respectively, in the opposite direction). As the time step of the simulations is 1 fs, this behavior persists over 5×10^4 time steps and turns out to be relatively robust owing to the complex time behavior of the system and to the atom-based algorithm that is employed. When averaging over longer periods, this effect is attenuated as shown

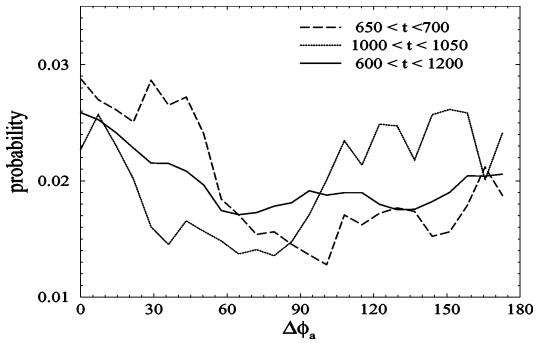

Figure 15. Probability distribution of $\Delta\phi_a$ averaged over time intervals $t \in$[650 ps, 700 ps] (dashed line), $t \in$[1000 ps, 1050 ps] (dotted line), and $t \in$[600 ps, 1200 ps] (full line).

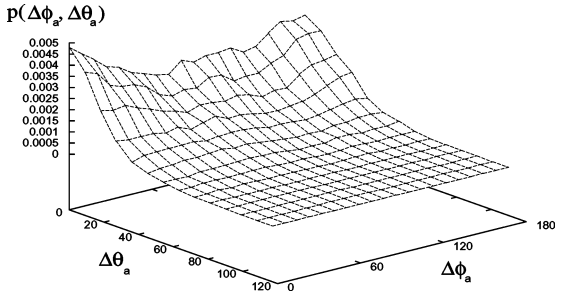

Figure 16. Average probability distribution function $p(\Delta\theta_a, \Delta\phi_a)$ obtained with $n = 50$ histogram bars and averaged over $t \geq 100$ ps. $\Delta\theta_a$ and $\Delta\phi_a$ are given in degrees.

in Figure 15 for time range $t \in$[600 ps, 1200 ps]. Owing to the values of the atom mobility and to their complex motion, we believe here that the orbit of the system visited a sufficiently large phase space volume for the curves of Figure 15 to constitute a reliable signature of the average spatial organisation of the surfactant chains in air. We thus believe that the larger probability for $\Delta\phi = 0$ when $t \in$[600 ps, 1200 ps] is reminiscent of the tendency of neighboring alkyl chains to preferentially have the same orientation. This effect is weak due to the large value of the molecular surface ($A = 0.64$ nm^2), and we expect it to sharpen for smaller surfaces and larger number of molecules.

Figure 16 shows the probability distribution $p(\Delta\theta_a, \Delta\phi_a)$ when averaging over the time range $t > \tau_r$. Two main features can be observed in this figure: first, the maximum at $(\Delta\theta_a, \Delta\phi_a) = (0, 0)$ indicates that neighboring alkyl vectors tend to be oriented in the same direction. This feature is coherent with the previously discussed role of Lennard-Jones and Coulomb potentials that tend to lock neighboring chains together. Second, another maximum at $(\Delta\theta_a, \Delta\phi_a) = (0, 180)$ indicates the existence of a second favored configuration where alkyl chains are antiparallel. Both peaks have probability $p(0, 0) \approx p(0, 180) \approx 5 \times 10^{-3}$. Between the latter, probability decreases down to $p(0, 90) \approx 3 \times 10^{-3}$, whereas for a given $\Delta\phi_a$ and varying values of $\Delta\theta_a$, the probability decreases as a Maxwellian law. From the point of view of hydrophobic steric interactions, the existence of two types of nearest neighbor configurations for the alkyl vectors will yield different intermolecular stresses in the vicinity of the chains. The broad shape of the maxima of Figures 15 and 16 is attributed to the finite velocity of the atoms. Thermal effects indeed promote disorder and compete with the tendency of the intermolecular potential to lock neighboring alkyl chains together. One consequence of this competition is that the system skips between oriented configurations for the alkyl vectors and disordered ones as time evolves.

7. Conclusions

The dynamics of a set of 40 monododecyl pentaethylene glycol surfactant molecules adsorbed on a sample of 2350 water molecules is investigated with the CFF91 force field. Surfactant molecules are close to dense packing, and all relevant degrees of freedom are included in the description for both surfactant and water molecules. Due to bond length dynamics and to the noise introduced in the NVT dynamics due to the direct numerical cutoff technique, mobility of the molecules is enhanced and relaxation to stationarity is eased. One first result of our investigations raises the issue of considering internal degrees of freedom and atom-based cutoff algorithms for nonbonded coupling when simulating surfactant molecules at water/air interfaces. The system shows a clear stationary behavior for simulation time $t > 600$ ps. In this regime, we show that the glycol polar headgroups of the surfactant molecules are not vertically anchored in water but are rather mobile and exhibit a tilted and entangled average behavior similar to the one of alkyl chains. The resulting surfactant monolayer is characterized by a complex molecular structure where both alkyl a glycol chains of the molecules have distorted geometries and large tilt angles. We show that the mass density profile across the interface consists of domains where water, glycol chain, and alkyl chain distributions strongly overlap. Mass density distributions allow the determination of the width of these distributions for surface coverage $A = 0.64$ nm^2 per molecule. Additional information about the interface structure is obtained from the probability distribution of polar and azimuth angle difference between nearest neighboring molecules. This distribution indicates that hydrophobic chains tend to lock together and develop a common oriented behavior driven by intermolecular coupling. The picture arising here is therefore a water/air interface that is neither a well-arranged monolayer nor a completely disordered system but rather an intermediate configuration characterized by highly entangled surfactant chains with reminiscent orientational order.

Acknowledgment. The authors thank Prof. A. Sanfeld and R. Brasseur for fruitful discussions, Dr. F. Chauvet for computational help, and all the members of the ESA topical team MAP for important seminal suggestions. J. Wescott is gratefully aknowledged for determinant help in the use of the Cerius^2 package. The CINES is also aknowledged for computational power and support. This work has been supported by ESA contract "FASES".

References and Notes

(1) Rehage, H. *Transport Mechanisms across Fluid Interfaces*; Dechema, Ed.; Wiley-VCH: Weinheim, 2000, Vol. 136, pp 3−44.
(2) Fainerman, V. B.; Miller, R.; Wustneck, R.; Makievski, A. V. *J. Phys. Chem.* **1996**, *100*, 7669.
(3) Liggieri, L.; Ferrari, M.; Massa, A.; Ravera, *F. Colloids Surf. A* **1999**, *156*, 455.
(4) Ravera, F.; Ferrari, M.; Miller, R.; Liggieri, L. *J. Phys. Chem. B* **2001**, *105*, 195.
(5) Karaborni, S.; Siepmann, J. I. *Mol. Phys.* **1994**, *83*, 345.
(6) Kuhn, H.; Rehage, H. *J. Phys. Chem. B* **1999**, *103*, 8493; Lu, J. R.; Li, Z. X.; Thomas, R. K.; Staples, E. J.; Thompson, L.; Tucker, I.; Penfold, J. *J. Phys. Chem.* **1994**, *98*, 6559.
(7) Lu, J. R.; Li, Z. X.; Thomas, R. K.; Binks, B. P.; Crichton, D.; Fletcher, P. D. I.; McNab, J. R.; Penfold, J. *J. Phys. Chem. B* **1998**, *102*, 5785.
(8) Lang, J. C.; Morgan, R. D. *J. Chem. Phys.* **1980**, *73*, 5849; Mitchell, D. J.; Tiddy, G. J. T.; Warring, L.; Bostock, T.; McDonald, M. P. *J. Chem. Soc., Faraday Trans. 1* **1983**, *79*, 975.
(9) Kuhn, H.; Rehage, H. *Tenside Surfactants Deterg.* **1998**, *35*, 448.
(10) Laaksonen, L.; Rosenholm, J. *Chem. Phys. Lett.* **1993**, *216*, 429.
(11) Paschek, D.; Engels, T.; Geiger, A.; von Rybinski, W. *Colloids Surf. A* **1999**, *156*, 489.

(12) Lu, J. R.; Li, Z. X.; Thomas, R. K.; Staples, E. J.; Thompson, L.; Tucker, I.; Penfold, J. *Langmuir* **1993**, *9*, 2417.
(13) Molecular Simulations Inc., Cerius2 Ver. 4.2, San Diego, 2000.
(14) Verlet, L. *Phys. Rev.* **1967**, *159*, 98.
(15) Allen, M. P.; Tildesley, D. J. *Computer Simulations of Liquids*; Clarenton Press: Oxford, 1987.
(16) Maple, J. R.; Wang, M. J.; Stockfisch, T. P.; Dinur, U.; Waldman, M.; Ewig, C. S.; Hagler, A. T. *J. Comput. Chem.* **1994**, *15*, 162.
(17) Francl, M. M., et al. *J. Chem. Phys.* **1982**, *77*, 3654.
(18) Dinur. U.; Hagler, A. T. *J. Chem. Phys.* **1989**, *91*, 2949.
(19) Dinur, U.; Hagler, A. T. New approaches to empirical force fields, in *Reviews of Computational Chemistry*, Lipkowitz, K. B.; Boyd, D. B., Eds. VCH: New York, 1991; Vol. 2, Chapter 4.
(20) Waldman, M.; Hagler, A. T. *J. Comput. Chem.* **1993**, *14*, 1077.
(21) Guillot, B. *J. Mol. Liq.* **2002**, *101*, 219.
(22) Berendsen, H. J. C.; Grigera, J. R.; Straatsma, T. P. *J. Phys. Chem.* **1987**, *91*, 6269.
(23) Bond coupling constant between hydrogen and oxygen atom of water molecules are $\alpha_i^{(b)} = 1126.56$ kcal/mol and $\alpha_j^{(\theta)} = 99.68$ kcal/mol.rad^2. Diagonal parameters of water nonbonded couplings are $r_{H,H}^{(0)} = 1.098$ Å, $\epsilon_{H,H} = 0.013$ kcal/mol for hydrogen and $r_{O,O}^{(0)} = 3.608$ Å, $\epsilon_{O,O} = 0.274$ kcal/mol for oxygen atoms.
(24) Floriani, E.; Mannella, R.; Grigolini, P. *Phys. Rev. E* **1995**, *52*, 5910; Torcini, A.; Antoni, M. *Phys. Rev. E* **1999**, *59*, 2746.
(25) Ewald, P. P. *Ann. d. Phys.* **1921**, *64*, 253.
(26) Greengard, L. *Science* **1994**, *265*, 909.
(27) Tuckerman, M.; Berne, B. J.; Martyna, G. J. *J. Chem. Phys.* **1992**, *97*, 1990; Komeiji, Y. *J. Mol. Struct.* **2000**, *530*, 237.
(28) For example, when considering carbon−carbon couplings one gets $\alpha_{C-C}^{(b)} = 599.3400$ kcal/mol/Å^2 and $\alpha_{C-C-C}^{(\theta)} = 79.0320$ kcal/mol/rad^2.
(29) Kalko, S.; Sese, G. *J. Chem. Phys.* **1996**, *104*, 9578; Sagui, C.; Darden, T. *Annu. Rev. Biophys. Biomol. Struct.* **1999**, *28*, 155.
(30) Lu, J. R.; Li, Z. X.; Su, T. J.; Thomas, R. K. *Langmuir* **1993**, *9*, 2408.
(31) Lu, J. R.; Simister, E. A.; Thomas, R. K.; Penfold, J. *J. Phys. Cond. Matter*. **1994**, *6*, A403.
(32) Lu, J. R.; Li, Z. X.; Thomas, R. K.; Staples, E. J.; Tucker, I.; Penfold, J. *J. Phys. Chem.* **1993**, *97*, 8012.
(33) Ichikawa, H.; Kameda, Y.; Yamaguchi, T.; Wakita, H.; Misawa, M. *Mol. Phys.* **1991**, *73*, 79.
(34) Molecules *k* and *j* are nearest neighbors if their relative distance at the interface height is minimal that is to say if distance $|r_{k,m_g} - r_{j,m_g'}|$ is minimal. For surfactant molecule *k* atom m_g is shown in Figure 10.